



LAWRENCE
LIVERMORE
NATIONAL
LABORATORY

Nonlinear ELM simulations based on a non-ideal peeling-ballooning model using the BOUT++ code

X. Q. Xu, B. Dudson, P. B. Snyder, M. V. Umansky, H. Wilson

January 6, 2011

Nuclear Fusion

Disclaimer

This document was prepared as an account of work sponsored by an agency of the United States government. Neither the United States government nor Lawrence Livermore National Security, LLC, nor any of their employees makes any warranty, expressed or implied, or assumes any legal liability or responsibility for the accuracy, completeness, or usefulness of any information, apparatus, product, or process disclosed, or represents that its use would not infringe privately owned rights. Reference herein to any specific commercial product, process, or service by trade name, trademark, manufacturer, or otherwise does not necessarily constitute or imply its endorsement, recommendation, or favoring by the United States government or Lawrence Livermore National Security, LLC. The views and opinions of authors expressed herein do not necessarily state or reflect those of the United States government or Lawrence Livermore National Security, LLC, and shall not be used for advertising or product endorsement purposes.

Nonlinear ELM simulations based on a non-ideal peeling-ballooning model using the BOUT++ code¹

X. Q. Xu¹, B. Dudson², P. B. Snyder³, M. V. Umansky¹ H. Wilson²

¹) Lawrence Livermore National Laboratory, Livermore, CA 94550 USA

²) University of York, Heslington, York YO10 5DD, UK

³) General Atomics, San Diego, CA 92186 USA

e-mail contact of main author: xxu@llnl.gov

Abstract. A minimum set of equations based on the Peeling-Ballooning (P-B) mode with non-ideal physics effects (diamagnetic drift, ExB drift, resistivity, and anomalous electron viscosity) is found to simulate pedestal collapse when using the BOUT++ simulation code, developed in part from the original fluid edge code BOUT. Linear simulations of peeling-ballooning modes find good agreement in growth rate and mode structure with ELITE calculations. The influence of the $E \times B$ drift, diamagnetic drift, resistivity, anomalous electron viscosity, ion viscosity, and parallel thermal diffusivity on peeling-ballooning modes is being studied; we find that (1) the diamagnetic drift and ExB drift stabilize the peeling-ballooning mode in a manner consistent with theoretical expectations; (2) resistivity destabilizes the peeling-ballooning mode, leading to resistive peeling-ballooning mode; (3) anomalous electron and parallel ion viscosities destabilize the peeling-ballooning mode, leading to a viscous peeling-ballooning mode; (4) perpendicular ion viscosity and parallel thermal diffusivity stabilize the peeling-ballooning mode. With addition of the anomalous electron viscosity under the assumption that the anomalous kinematic electron viscosity is comparable to the anomalous electron perpendicular thermal diffusivity, or the Prandtl number is close to unity, it is found from nonlinear simulations using a realistic high Lundquist number that the pedestal collapse is limited to the edge region and the ELM size is about 5-10% of the pedestal stored energy. This is consistent with many observations of large ELMs. It is also shown that for high Lundquist number there are two distinct processes in the evolution of pressure profiles: a fast collapse greatly flattening the pressure profile near the peak pressure gradient on the order of tens of Alfvén times after the onset of nonlinear P-B mode and a slow buildup of pressure gradient. We can characterize the fast collapse as a magnetic reconnection triggered by P-B modes \rightarrow an island formation and magnetic braiding \rightarrow bursting process and a slow collapse as a turbulence transport process. The estimated island size is consistent with the size of fast pedestal pressure collapse. In the stable α -zones of ideal P-B modes, nonlinear simulations of viscous ballooning modes or current-diffusive ballooning mode (CDBM) for ITER H-mode scenarios are presented.

1. Introduction

Through the development of the theory of peeling-ballooning (P-B) modes and their numerical implementation in codes such as ELITE [1, 2], a robust prediction of edge MHD stability limits is available for existing and future tokamaks. It has been found that large ELMs are triggered and pedestal height is constrained by the ideal P-B stability. P-B modes are ideal MHD modes which are driven by a combination of sharp pressure gradients (ballooning) and bootstrap current in the pedestal. The onset of each ELM (type-I) has been consistently found to correlate with crossing of the ideal P-B stability boundary [3], i.e., P-B theory

¹This work was performed for USDOE by LLNL under Contract DE-AC52-07NA27344, grants DE-FG03-95ER54309 at general Atomics, and by the UK Engineering and Physical Sciences Research Council under grant EP/H012605/1 and the Euro. Commun. under the contract of Association between EURATOM and CCFE.

successfully describes the trigger of the ELM. Having said this, there are situations where the profiles sit at marginal stability for some time before the ELM is triggered [4], so linear stability analysis may not provide the complete picture. The nonlinear dynamics, and in particular the physics of the ELM energy loss and pedestal dynamics after the onset of each ELM (type-I) remain uncertain, and may even play some role in the trigger.

Nonlinear ELM simulations become computationally difficult for high Lundquist number due to the fine resolution needed to resolve the narrow current sheet at rational surfaces and/or narrowing fingers as a result of explosive ideal MHD instabilities predicted from nonlinear ballooning theory [5, 6, 7], leading to collapse of the simulation time-step at the early non-linear stage of P-B mode development[6]. A common practice is to use an anomalous resistivity and/or ion viscosity as well as parallel thermal diffusivity to achieve nonlinear ELM simulations, which leads to significantly different linear growth rates and instability thresholds. Furthermore, in nonlinear resistive MHD simulations, the pedestal pressure collapses deep into the plasma core, which yields much larger ELM sizes than observed.

In this paper we summarize recent developments in nonlinear simulations of peeling-ballooning modes with anomalous electron viscosity and explore its role in ELM crashes[8, 9]. From nonlinear simulations we have found that the P-B modes trigger magnetic reconnection, which drives the collapse of the pedestal pressure. The hyper-resistivity is found to limit the radial spreading of ELMs by facilitating magnetic reconnection. In quiescent H-mode plasma, the hyper-resistivity also drives the viscous ballooning mode or the so-called current diffusive ballooning mode (CDBM)[10], which is a magnetohydrodynamic (MHD) instability and localizes in the outer region of the torus where the gradient of the pressure aligns with the magnetic curvatures.

The organization of this paper is as follows. The basic set of equations and simulation model are given in Sect. 2. Nonlinear simulations of peeling-ballooning modes are described in Sect. 3. Nonlinear CDBM turbulence simulations in ITER H-mode Scenarios are given in Sect. 4. The results are summarized and discussed in Sect. 5.

2. A Non-Ideal MHD Simulation Model

In the present paper, we describe nonlinear simulations of plasma edge pedestal collapse using a three-field model in the tokamak configuration. The simulations are carried out in the BOUT++ two-fluid framework [11], which allows studies of nonlinear dynamics of ELMs including extensions beyond MHD physics. Based on the P-B model with non-ideal physics effects (diamagnetic drift, ExB drift, resistivity, anomalous viscosity and parallel thermal diffusivity), a minimum set of nonlinear equations for perturbations of the magnetic flux A_{\parallel} , electric potential ϕ , and pressure P can be extracted from a complete set of the BOUT two-fluid equation [14], with an additional effect of hyper-resistivity incorporated [15]. This can be written as

$$\frac{\partial \varpi}{\partial t} + \mathbf{v}_{\mathbf{E}} \cdot \nabla \varpi = B_0 \nabla_{\parallel} J_{\parallel} + 2\mathbf{b}_0 \times \kappa_0 \cdot \nabla P + \mu_{i,\parallel} \nabla_{\parallel}^2 \varpi + \mu_{i,\perp} \nabla_{\perp}^2 \varpi \quad (1)$$

$$\frac{\partial P}{\partial t} + \mathbf{v}_{\mathbf{E}} \cdot \nabla P = \chi_{\parallel} \nabla_{\parallel}^2 P \quad (2)$$

$$\frac{\partial A_{\parallel}}{\partial t} = -\nabla_{\parallel} \Phi + \frac{\eta}{\mu_0} \nabla_{\perp}^2 A_{\parallel} - \frac{\eta_H}{\mu_0} \nabla_{\perp}^4 A_{\parallel} \quad (3)$$

$$\begin{aligned}\varpi &= \frac{n_0 M_i}{B_0} \left(\nabla_{\perp}^2 \phi + \frac{1}{n_0 Z_i e} \nabla_{\perp}^2 P \right), \Phi = \phi + \Phi_0, \\ J_{\parallel} &= J_{\parallel 0} - \frac{1}{\mu_0} \nabla_{\perp}^2 A_{\parallel}, v_E = \frac{1}{B_0} (b_0 \times \nabla_{\perp} \Phi).\end{aligned}$$

Here $\nabla_{\parallel} F = B \partial_{\parallel} (F/B)$ for any F , $\partial_{\parallel} = \partial_{\parallel}^0 + \tilde{\mathbf{b}} \cdot \nabla$, $\tilde{\mathbf{b}} = \tilde{\mathbf{B}}/B = \nabla_{\parallel} A_{\parallel} \times \mathbf{b}_0/B$, $\partial_{\parallel}^0 = \mathbf{b}_0 \cdot \nabla$, $\kappa_0 = \mathbf{b}_0 \cdot \nabla \mathbf{b}_0$. Although hyper-resistivity η_H , also known as electron viscosity, is generally negligibly small in collisional plasmas, it can be significant in a collisionless plasma. In this model the frozen-in flux constraint of ideal MHD theory is broken by either resistivity or hyper-resistivity. To investigate the effect of transport on the peeling-ballooning stability, the parallel thermal diffusivity χ_{\parallel} , anomalous parallel and perpendicular ion viscosities ($\mu_{i\parallel}$ and $\mu_{i\perp}$) are also included. However, unless specified, all transport terms — viscosities, thermal diffusivity, hyper-resistivity, etc. — are zero.

The equations (1)-(3) are solved using a field-aligned (flux) coordinate system (x, y, z) with shifted radial derivatives [11]. Differencing methods used are 4th-order central differencing and 3rd-order WENO advection scheme. The resulting difference equations are solved with a fully implicit Newton-Krylov solver: Sundials CVODE package. Radial boundary conditions used are: $\varpi = 0$, $\nabla_{\perp}^2 A_{\parallel} = 0$, $\partial P / \partial \psi = 0$, and $\partial \phi / \partial \psi = 0$ on the inner radial boundary; $\varpi = 0$, $\nabla_{\perp}^2 A_{\parallel} = 0$, $P = 0$, and $\phi = 0$ on outer radial boundary. The domain is periodic in the parallel coordinates y (with a twist-shift condition) and in z (toroidal angle). For efficiency, when performing nonlinear simulations, only 1/5th of the torus is simulated. The number of grid cells in each coordinate are $n_{\psi} = 512$, $n_{\theta} = 64$, $n_{\zeta} = 32$ for linear runs and $n_{\zeta} = 64, 128, 256$ for nonlinear runs (n_{ψ} and n_{θ} are kept fixed).

In this study, the resistivity η , hyper-resistivity η_H , ion viscosities ($\mu_{i\parallel}$ and $\mu_{i\perp}$), parallel thermal diffusivity χ_{\parallel} and edge density $n_0 = 1 \times 10^{19} m^{-3}$ are treated as constants in space-time across the simulation domain. In the present simplified model, both equilibrium flow and turbulent zonal flow have been set to be zero: $\mathbf{V}_0 = \mathbf{V}_{E0} + \mathbf{V}_{\nabla P_i} = 0$ and $\langle \delta \mathbf{v} \rangle_{\zeta} = \langle \mathbf{v}_E \rangle_{\zeta} + \langle \mathbf{v}_{\nabla P_i} \rangle_{\zeta} = 0$. Therefore, the equilibrium electric field is $E_{r0} = (1/n_0 Z_i e) \nabla_r P_{i0}$ with ion pressure $P_{i0} = P_0/2$, and the perturbed electric field is $\langle E_r \rangle_{\zeta} = (1/n_0 Z_i e) \nabla_r \langle P_i \rangle_{\zeta}$. The zonal magnetic field is also set to be zero as it is negligibly small compared to the equilibrium magnetic field B_0 .

3. Nonlinear Simulations of Peeling-Ballooning Modes in Circular Geometry

To study the physics of nonlinear P-B mode dynamics, we choose circular cross-section toroidal equilibria with an aspect ratio of 2.9 generated by the TOQ equilibrium code. Two model equilibria have been simulated for H-mode plasmas with steep pressure and current gradients at the edge [16]. The first equilibrium (cbm18_dens8), which we describe in some detail here, is far from the marginal P-B instability threshold with a pedestal toroidal pressure $\beta_{t0} = 1.941 \times 10^{-2}$ and a normalized pedestal width $L_{ped}/a = 0.0486$. We have also considered a second equilibrium (cbm18_dens6) that is near the marginal P-B instability threshold with $\beta_{t0} = 1.45 \times 10^{-2}$ and $L_{ped}/a = 0.0518$. Results for that case are described in [8], and will not be discussed here. Parameters that are held fixed in the simulations include a minor radius $a = 1.2\text{m}$, major radius $R_0 = 3.4\text{m}$, toroidal field on axis $B_0 = 2T$, an edge $q_a \simeq 3$, the pedestal pressure 2/3 of the axis pressure, and a pedestal half width 7% of the poloidal flux.

A series of BOUT++ simulations is conducted to investigate the scaling characteristics of the P-B mode in the strongly unstable case as a function of two dimensionless quantities S and S_H [8]. One is a S -scan for a fixed $S_H = 10^{12}$, while the other is a S_H -scan for a fixed $S = 10^7$ or $S = 10^8$. Here the Lundquist number $S = \mu_0 R_0 v_A / \eta$ is the dimensionless ratio of an Alfvén wave crossing timescale to a resistive diffusion timescale of magnetic field, v_A is the Alfvén velocity, η resistivity, and R the major radius. Similarly, the hyper-Lundquist number $S_H = \mu_0 R_0^3 v_A / \eta_H = S / \alpha_H$ is the dimensionless ratio of an Alfvén wave crossing timescale to a hyper-resistive current diffusion timescale, with a dimensionless hyper-Lundquist parameter $\alpha_H = \eta_H / R_0^2 \eta$. For a collisional electron viscosity, $\alpha_H \simeq \mu_e / R_0^2 \nu_{ei}$. Assuming that the anomalous kinematic electron viscosity μ_e is comparable to the anomalous electron thermal diffusivity χ_e , for edge plasma parameters $\mu_e \simeq \chi_e \simeq 1 m^2/s$ and electron-ion collision frequency $\nu_{ei} \simeq 10^5/s$, we can estimate the amplitude of the hyper-Lundquist parameter to be $\alpha_H \simeq 10^{-4} - 10^{-6}$.

3.1 Linear Simulations

3.1.1 Linear benchmarking

Linear simulations of P-B mode evolution find good agreement in growth rate and mode structure with ELITE calculations [2, 11]. Fig. 1 shows the growth rate vs toroidal mode number n of the strongly unstable equilibrium as calculated by BOUT++ for various cases. A good agreement for an ideal MHD model is shown between GATO (open circle), ELITE (open triangle), and BOUT++ (black curve with filled circle). The influence of the $E \times B$ drift, diamagnetic drift, resistivity, and anomalous electron viscosity (hyper-resistivity) on linear P-B modes has been studied. We find that (1) the diamagnetic drift and ExB drift stabilize the P-B mode (red and blue filled circle) in a manner consistent with theoretical expectations [12, 13]; (2) resistivity destabilizes the P-B mode, leading to resistive P-B mode (green cross) for $S = 10^5$ and $S_H = \infty$; (3) anomalous electron viscosity destabilizes the P-B mode, leading to a viscous P-B mode (purple open square) for a fixed $S = 10^8$ and $\alpha_H = 10^{-4}$. For a fixed $S = 10^8$, as α_H reduces from 10^{-4} to 10^{-6} , both resistive and viscous effects disappear. The BOUT++ reduced-MHD model captures the marginal stability value $n > 3$.

3.1.2 The effect of transport coefficients on linear instabilities

In nonlinear simulations, the stability of P-B mode is often evaluated with transport coefficients where plasma profiles are evolving as in real experiments. Therefore the effect of transport coefficients on linear stability analysis should be assessed. The coefficients under discussion are only the diagonal elements of the transport matrix, such as viscosities, thermal diffusivity, and hyper-resistivity. The effect of hyper-resistivity is discussed in sect. 3.1.1. The parallel thermal diffusivity χ_{\parallel} is typically in kinetic regime inside the pedestal and in the collisional regime in the Scrape-Off-Layer. While the ion viscosities are typically caused by fluctuations, and can be obtained by renormalizing the nonlinear interaction with background turbulence.

Figure 2 shows the dependence of the growth rate on thermal diffusivity, the perpendicular and parallel ion viscosities for mode $n=15$ with the $E \times B$ drift and diamagnetic drift, $S = 10^8$ and $\alpha_H = 10^{-4}$. The other parameters are the same as in Fig. 1. The general trend is that the

thermal diffusivity and ion perpendicular viscosity stabilize the P-B mode, while the parallel ion viscosity destabilizes the P-B mode. When the parallel thermal diffusivity $\chi_{\parallel} \gtrsim 10D_A$ where $D_A = R^2/\tau_A = 3.3 \times 10^8 m^2/s$ and $\tau_A = R/V_A$ is the Alfvén time, the growth rate of peeling-ballooning modes is significantly reduced. With increasing χ_{\parallel} , the parallel mode structure becomes more flute-like and the radial mode profile has narrowing finger structures on top of the usual Gaussian-like shape peaked at the maximum pressure gradient location. An important consideration when interpreting the results presented in Fig.2a) is theoretical models used to estimate pedestal parallel heat diffusivity χ_{\parallel} . In terms of Spitzer-Harm parallel heat diffusivities, $\chi_{e,\parallel}^{SH} \simeq 3.2v_{Te}\lambda_{ei}$, while for a heat flux limiting model, $\chi_{e,\parallel}^{FL} \simeq v_{Te}q_{95}R$. Here v_{Te} is the electron thermal speed, $\lambda_{ei} = v_{Te}\tau_{ei}$ the electron thermal mean free path and $\tau_{ei} \propto v_{Te}^3$ the collisional time for electron-ion Coulomb scattering evaluated at the thermal speed. For typical pedestal plasma parameters, $T_{e,ped}=1.0\text{keV}$, $n_{e,ped} = 2 \times 10^{-19}/m^3$, $q_{95}=4$, $\chi_{e,\parallel}^{FL} \simeq 0.55D_A$, the growth rate is reduced by 26% due to parallel heat conduction. For the same parameters, $\chi_{e,\parallel}^{SH} \simeq 1.53 \times 10^{10} m^2/s$ and $\chi_{e,\parallel}^{SH}/D_A \simeq 50$, the the growth rate is significantly reduced. For ITER pedestal parameters $T_{e,ped} \simeq 4.5\text{keV}$, $n_{e,ped} \simeq 5 \times 10^{-19}/m^3$, $\chi_{e,\parallel}^{SH} \simeq 2.62 \times 10^{11} m^2/s$ and $\chi_{e,\parallel}^{SH}/D_A \simeq 794$, while $\chi_{e,\parallel}^{FL} \simeq v_{Te}q_{95}R \simeq 1.16D_A$. Similarly, for typical pedestal plasma parameters, $\mu_{i\perp} \simeq (0.1 - 1)m^2/s$ as radial thermal diffusivity with the assumption that the Prandtl numbers are close to unity, namely, $\mu_{e,\perp}/\chi_{e,\perp} \sim \mu_{i,\perp}/\chi_{i,\perp}$ and $\chi_{e,\perp} \simeq \chi_{i,\perp}$, which yields $\mu_{i\perp}/D_A \simeq (0.3 - 3) \times 10^{-8}$, the impact of the perpendicular ion viscosity on the growth rate is negligible small.

3.2 Role of the hyper-resistivity on nonlinear simulations

Nonlinear simulations of P-B modes at the early non-linear stage of development reveal that the current sheet narrows with increasing Lundquist numbers. For typical pedestal plasma parameters, the Lundquist number is around $S \simeq 10^8 - 10^{10}$, the growth rate of the P-B mode is around $\gamma_{PB} \simeq 0.1\omega_A$, and the width of the resistive current sheet $\Delta_J \simeq R\sqrt{\omega_A/\gamma_{PB}/S}$ is around 10-100 microns, which is comparable to be electron Larmor radius ρ_e . In the absence of the hyper-resistivity, the simulation time-step collapses as the radial scale-length of the current sheet approaches the radial grid spacing Δ_x for typical resistive MHD simulations $\Delta_x \gg \Delta_J \simeq \rho_e$. With the hyper-resistivity, the width of the hyper-resistive current sheet is $\Delta_H \simeq R(\omega_A/\gamma_{PB}/S_H)^{1/4}$. The hyper-resistivity could arise, for example, from small scale electron turbulence in the H-mode pedestal [17]. For the rest of this paper, we assume $S_H = 10^{12}$; hence $\Delta_H (\simeq 1.78\text{mm}) > \Delta_x (\simeq 1.1\text{mm}) \gg \Delta_J$ with $\Delta_H/\Delta_J > 17.8$.

The radial pressure profiles at the outer mid-plane at several different time slices and different Lundquist numbers are shown in Figure 3. It is clearly shown that the pedestal pressure collapses deeply inside the core plasma at low Lundquist number ($S = 10^5$). It is also shown that for high Lundquist number there are two distinct processes in the evolution of pressure profiles: a fast collapse greatly flattening the pressure profile near the peak pressure gradient on the order of tens of Alfvén times after the onset of nonlinear P-B mode, $t = 74\tau_A$, and a subsequent slow buildup of pressure gradient. We can characterize the fast collapse as a magnetic reconnection (triggered by P-B modes) \rightarrow an island formation \rightarrow bursting process, and a slow buildup as a turbulence transport process. The radial-poloidal pressure profiles clearly show the characteristics of the ballooning mode. As is well known from linear instability analysis, ϕ and A_{\parallel} have ballooning parity for the P-B mode. In the nonlinear stage, however, tearing parity component appears due to the nonlinear mode coupling, which

facilitates magnetic reconnection and island formation.

3.3 ELM-size

Defining an ELM size as $\Delta_{ELM}^{th} = \Delta W_{PED}/W_{PED} = \langle \int_{R_{in}}^{R_{out}} \oint dRd\theta (P_0 - \langle P \rangle_\zeta) \rangle_t / \int_{R_{in}}^{R_{out}} \oint dRd\theta P_0$, the ratio of the ELM energy loss (ΔW_{PED}) to the pedestal stored energy W_{ped} ($W_{ped} = 3/2 P_{ped} V_{plasma}$), the ELM size can be calculated from each nonlinear simulation. Here P is the pedestal pressure and the symbol $\langle \rangle_t$ means the average over time ($\sim 50 - 100\tau_A$) and symbol $\langle \rangle_\zeta$ means the average over bi-normal periodic coordinate. The lower integral limit is the pedestal inner radial boundary R_{in} , while the upper limit is the radial position of the peak pressure gradient R_{out} . Alternatively, the ELM size Δ_{ELM} can be calculated by radially integrating the pressure profile at the outer mid-plane as done in experiments, which is about a factor of two larger than that based on the 2D integral with ballooning characteristics: $\Delta_{ELM} \simeq 2\Delta_{ELM}^{th}$. The ELM size scaling vs. Lundquist number S is given in Fig. 4, which plots the ELM loss fraction $\Delta W_{ped}/W_{ped}$ as a function of the Lundquist number for a fixed $S_H = 10^{12}$. The size of the ELM eruption varies dramatically between the high and low resistivity cases. As the Lundquist number S is increased, the loss of thermal energy during the ELM drops from $\sim 50\%$ to $\sim 10\%$ over a range of $S = 10^4 - 10^7$ and then stays independent of S . This is due to the transition of dominance over resistance in Ohm's law, $\eta J \rightarrow \eta_H \nabla_\perp^2 J$ and therefore leads to a significant reduction of the inward spreading of the perturbed magnetic field from the region of the P-B drive (peak gradient region). For better convergence, a small parallel diffusion term is added to Eq. (2) for $S = 10^{10}$. A large resistivity ($S \propto \eta^{-1}$) yields a large ELM size, which is contradictory to experimental observations in many devices that the relative ELM size scales inversely with pedestal collisionality [18]. However with a fixed hyper-resistivity $S_H = 10^{12}$, when $S > S_c = \sqrt{S_H \omega_A / \gamma} > 10^6$, which is relevant to today's modestly sized tokamaks and ITER, the ELM size is insensitive to the resistivity.

Furthermore the ELM size is found to be proportional to the hyper-resistivity. If we assume that the hyper-resistivity scales inversely with pedestal collisionality ($\eta_H \propto \nu_{ei}^{-\nu}, \nu > 0$), then the ELM size scales inversely with pedestal collisionality, which is consistent with experiments in the high Lundquist number regime. In this regard, the hyper-resistivity induced either by dissipative driftwave/electron-temperature-gradient driven modes or electron transport in the presence of stochastic magnetic field in the collisional regime may yield a consistent collisionality.

4. Nonlinear Turbulence Simulations in ITER H-mode Scenarios

To study the physics of nonlinear P-B mode dynamics in x-point divertor geometry, we chose a toroidal equilibrium with an elongated cross-section and triangularity from one of the latest designs of the ITER 15 MA inductive H-mode scenario (under the burning condition) generated by the CORSICA equilibrium code [19]. Parameters are: minor radius $a = 2\text{m}$, major radius $R_0 = 6.2\text{m}$, toroidal field on axis $B_0 = 5.3\text{T}$, edge $q_{95} \simeq 3.2$, poloidal beta $\beta_{t0} = 3.4 \times 10^{-3}$ and $L_{ped}/a = 0.0076$, edge elongation $\kappa_{95} = 1.7$, and triangularity $\delta_{95} = 0.349$. Because of the relatively low pedestal height, the P-B mode is stable for this ITER H-mode plasma. In turn, we investigate current-diffusive ballooning mode (CDBM) [10]. The CDBM is destabilized by the current diffusion (i.e., the anomalous electron viscosity or hyper-resistivity) and has more impact in the stable α -zones of ideal ballooning mode.

Here $\alpha = -q^2 R d\beta/dr$, $\beta = P/2\mu_0 B_0^2$. It is precisely the same physics which limits the radial spreading of ELMs by facilitating magnetic reconnection when P-B modes are dominantly unstable. The original three-field CDBM model also includes anomalous perpendicular ion viscosity $\mu_{i,\perp}$ and thermal diffusivity χ_\perp , which provide stabilizing effect on the CDBM. Here we neglect these because nonlinear CDBM itself should provide the thermal transport to stabilize the CDBM, and the balance between the instability drive from current diffusion and the sink from self-consistent turbulent transport should determine the pedestal width.

BOUT++ simulations were carried out for CDBM turbulent transport, including the pedestal region that extends across the separatrix into the scrape-off layer (SOL) and private flux region. With poloidal flux, ψ , normalized to unity on the separatrix, we take the inner simulation boundary condition to be $\psi_c = 0.85$ and the outer boundary at $\psi_w = 1.05$. The toroidal segment is typically one fifth of the torus with full poloidal cross section. Radial boundary conditions used at $\psi = \psi_c$ and at $\psi = \psi_w$ are: $\varpi = 0$, $\nabla_\perp^2 A_\parallel = 0$, $\partial P/\partial\psi = 0$, and $\partial\phi/\partial\psi = 0$ on the inner radial boundary $\psi = \psi_c$; $\varpi = 0$, $\nabla_\perp^2 A_\parallel = 0$, $P = 0$, and $\phi = 0$ on the outer radial boundary $\psi = \psi_w$. Other boundary conditions are: sheath boundary conditions in y in the SOL and the private flux regions at the divertor plates, twist-shifted periodic in y in the closed flux region due to the choice of field-aligned coordinates, and periodic in z . For simplicity, the insulating divertor plate boundary conditions are used, i.e. all fluctuating variables are set to zero. In addition, our model used here includes parallel heat conduction in order to study the end-loss at the divertor plates. The parallel heat diffusivity follows the electron Braginskii value in the SOL and is set as a constant inside the separatrix, a ceiling for the heat flux at roughly the level of the free streaming flux ($\chi_\parallel \simeq v_{te} q_{95} R$) when kinetic effect is believed to be important. The number of grid cells in each coordinate are $n_\psi = 256$, $n_\theta = 128$, and $n_\zeta = 64$. The small parallel ion viscosity ($\mu_{\parallel i} \simeq 0.01\omega_A R^2$) is used for numerical convergence and its negligible effect on instability has been checked as shown in Fig. 2c).

The linear growth rate of CDBM modes vs toroidal mode number n is shown in Figure 5(a) with diamagnetic drift and ExB drift. The solid curve is the growth rate γ and dot-dashed curve is the frequency ω . The unstable spectrum is similar to P-B mode with growth rate peaked at $n=20$. The mode frequency linearly increases with mode number n . The hyper-resistivity dependence of the growth rate with mode number $n=15$ is shown in Fig. 5(b). The solid curve is the growth rate γ and dashed curve is the frequency ω . The dot-dashed curve is proportional to $\alpha_H^{1/5}$, which is an analytical estimate in strong ballooning limit with circular cross-section [10].

Nonlinear simulations of the CDBM are shown in Fig. 6 for ITER H-mode plasma. Figure 6(a) shows linear growth and nonlinear saturation of the CDBM. Figure 6(b) shows various pressure profiles. The black dotted curve is the initial pressure profile P_0 while the red dashed curve is the final pressure profile $P = P_0 + \delta p_{n=0}$, where $\delta p_{n=0}$ means the component of perturbed pressure δp with toroidal mode number $n=0$. The pink curve is the perturbed pressure $\langle\delta p\rangle_{rms}$, where $\langle\delta p\rangle_{rms}$ represents the root-mean-square average over bi-normal coordinate z . The blue curve is the relative pressure fluctuation $\langle\delta p\rangle_{rms}/P$. The initial peak pressure gradient is located at the normalized $\hat{\psi} = 0.984$. From the nonlinear simulations, we observe the following interesting features. The pressure P gradient drops from initial one P_0 by 31% as a result of CDBM driven radial transport. There is a broad radial profile of perturbed pressure $\langle\delta p\rangle_{rms}$ (red solid curve), indicating more inward turbulent spreading than outward

from its linear instability drive at $\hat{\psi} = 0.984$ for H-mode plasma. The relative pressure fluctuation peaks in the SOL due to relatively low pressure there. Figure 7 demonstrates the pressure perturbation on a poloidal slice (ψ, θ) at a fixed toroidal angle ζ in nonlinear phase, showing the characteristics of a ballooning mode and highly elongated turbulent structure away from the outboard midplane due to large x-point shear.

5. Summary

In conclusion, it is found from nonlinear simulations that the P-B modes trigger magnetic reconnection, which drives the collapse of the pedestal pressure. The anomalous electron viscosity or hyper-resistivity, is found to limit the radial spreading of the ELMs by facilitating magnetic reconnection. In addition, current diffusion drives the viscous ballooning modes or CDBM in the stable α -zones of ideal ballooning mode. The influence of the parallel thermal diffusivity and ion viscosity on the peak linear growth rate of peeling-ballooning modes is found within 30% for typical ranges of pedestal plasma parameters. The care must be taken when using Spitzer-Harm parallel thermal diffusivity for pedestal plasmas since the linear growth of peeling-ballooning modes can be significantly reduced or suppressed.

Acknowledgments

The authors wish to acknowledge T. Casper to provide ITER data.

References

- [1] H. R. Wilson *et al*, Phys. Plasmas 9 (2002) 1277.
- [2] P. B. Snyder *et al*, Phys. Plasmas 9 (2002) 2037.
- [3] P. B. Snyder *et al*, Nucl. Fusion 49 (2009).
- [4] H. Zohm *et al*, 37th EPS Conference on Plasma Phys. Hersonissos, 21 - 25 June 2010.
- [5] H. R. Wilson *et al*, Phys. Rev. Lett. **92**, 175006 (2004)
- [6] P. B. Snyder *et al*, 2005 Phys. Plasmas 12 056115
- [7] P. Zhu., C. .C .C. Hegna, C.R.Sovinec, *et al*, 2007 Phys. Plasmas 14 055903
- [8] X. Q. Xu *et al*, Phys. Rev. Lett. **105**, 175005 (2010).
- [9] B. D. Dudson,*et al*, submitted to Plasma Phys. Control. Fusion 2010.
- [10] M. Yagi *et al* 1993 Phys. Fluids B 5 3702
- [11] B. D. Dudson, H. R. Wilson, M. V. Umansky, X. Q. Xu, P. B. Snyder, Comput. Phys. Comm.,**180**, 1467 (2009).
- [12] K. V. Roberts and J. B. Taylor, Phys. Rev. Lett. **8**, 197 (1962).
- [13] W. M. Tang, R. L. Dewar, and J. Manickam, Nucl. Fusion **22**, 1079 (1982).
- [14] X. Q. Xu *et al*, Comm.in Comput.Phys.4,949(2008).

- [15] P. K. Kaw *et al*, Phys. Rev. Lett. **43**, 1398 (1979).
- [16] B. J. Burke *et al*, Phys. Plasmas **17**, 032103 (2010).
- [17] P. H. Diamond, private communication, 2010.
- [18] A. Loarte, G. Saibene, R. Sartori *et al*, 2003 Plasma Phys. Control. Fusion **45** 1549.
- [19] T. Casper, Y. Gribov, A. Kavin *et al*, 23rd IAEA Fusion Energy Conference, 11-16 October 2010 Daejeon, Republic of Korea, <http://www-pub.iaea.org/MTCD/Meetings/cn180-papers.asp>, ITR/P1-19.

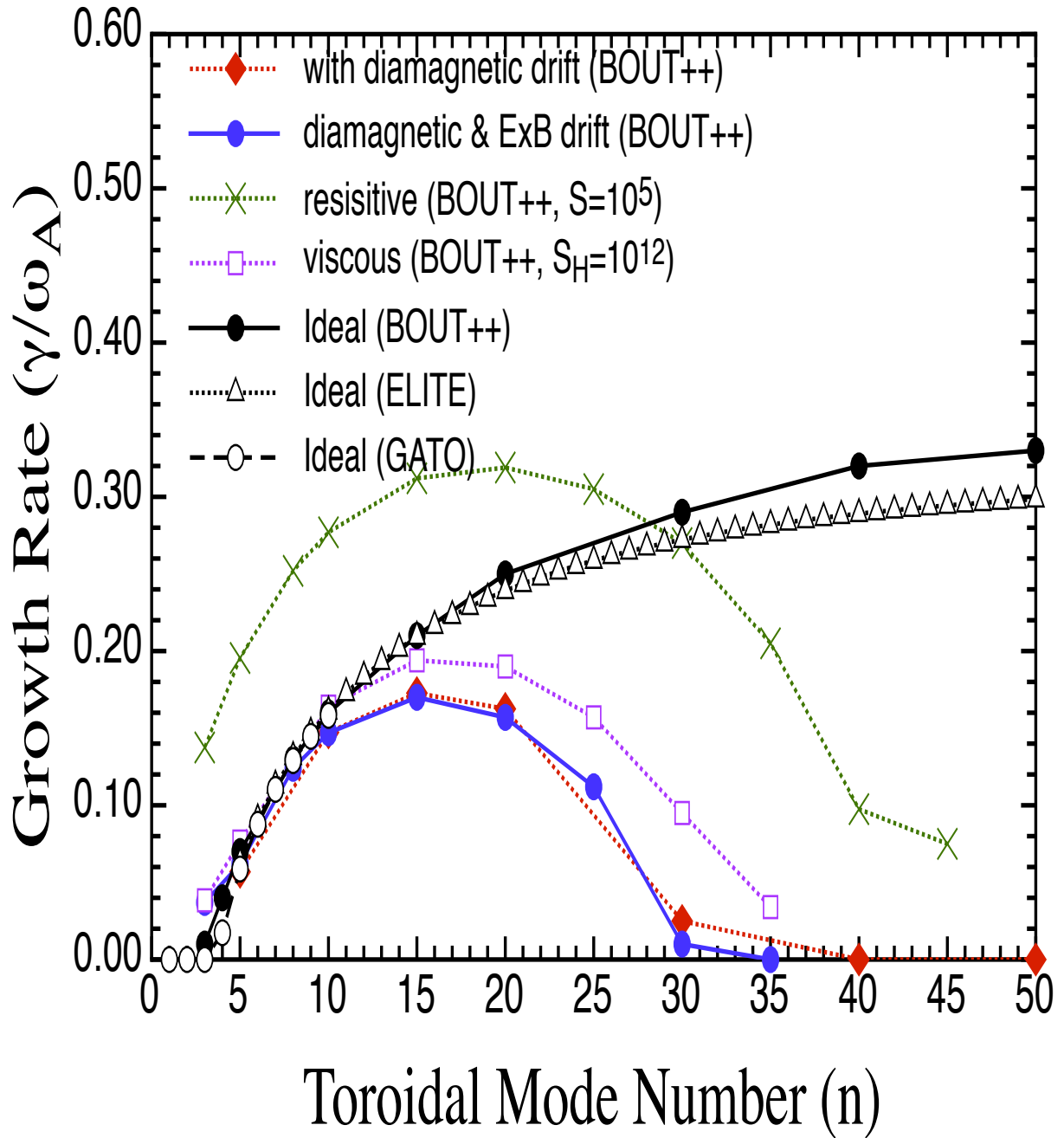


FIG. 1: The influence of the non-ideal physics on the linear growth rate of peeling-ballooning modes vs toroidal mode number n for the ideal MHD peeling-ballooning mode (black), with diamagnetic drift stabilization (red), with ExB drift stabilization (blue), resistive (green cross) and viscous (purple square) peeling-ballooning mode.

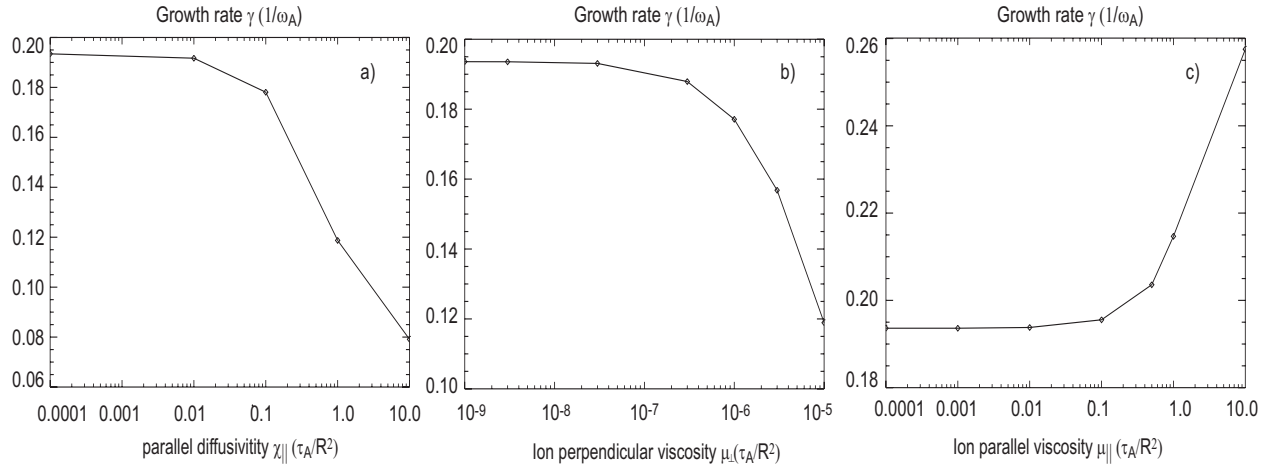


FIG. 2: The growth rate of the $n = 15$ eigenmode vs various transport coefficients with the $E \times B$ drift and diamagnetic drift for $S = 10^8$ and $\alpha_H = 10^{-4}$: (a) the parallel diffusivity $\chi_{||}$, (b) the ion perpendicular viscosity $\mu_{i,\perp}$ and (c) the ion parallel viscosity $\mu_{i,||}$.

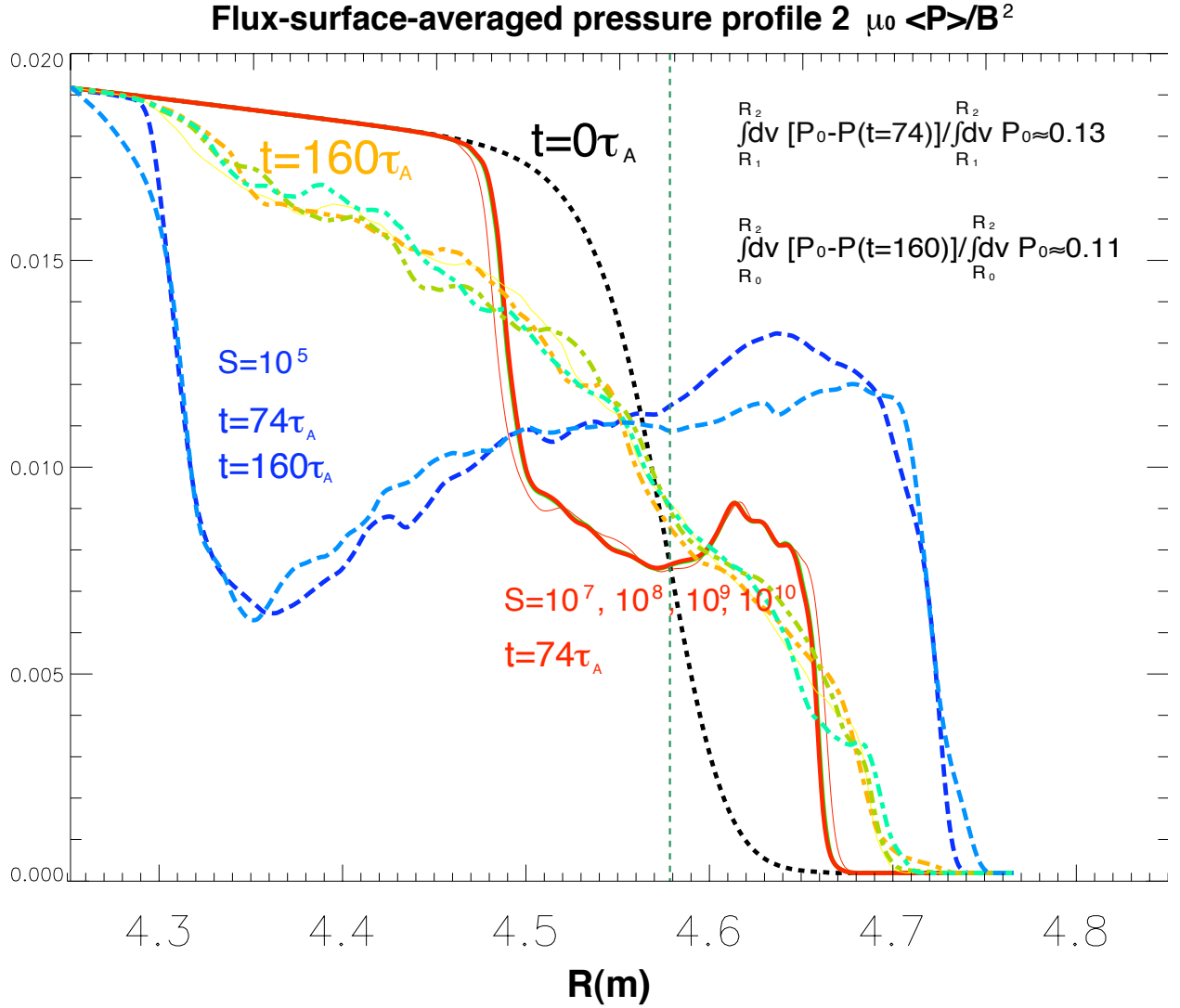


FIG. 3: Reproduced from X.Q.Xu et al, Fig. 2 [1] with courtesy of Physical Review Letter. Radial pressure profiles at several different Lundquist numbers S and 4 time slices ($t=0, 74, 160\tau_A$). The black dotted line is at $t=0$; blue dashed group lines for $S = 10^5$ at $t=74\tau_A$ and $160\tau_A$; red solid group lines for $S = (10^7, 10^8, 10^9, 10^{10})$ at $t=74\tau_A$; yellow dotted-dashed group lines for $S \geq 10^7$ at $t=160\tau_A$. The vertical line indicates the position of peak pressure gradient. Here $S_H = 10^{12}$.

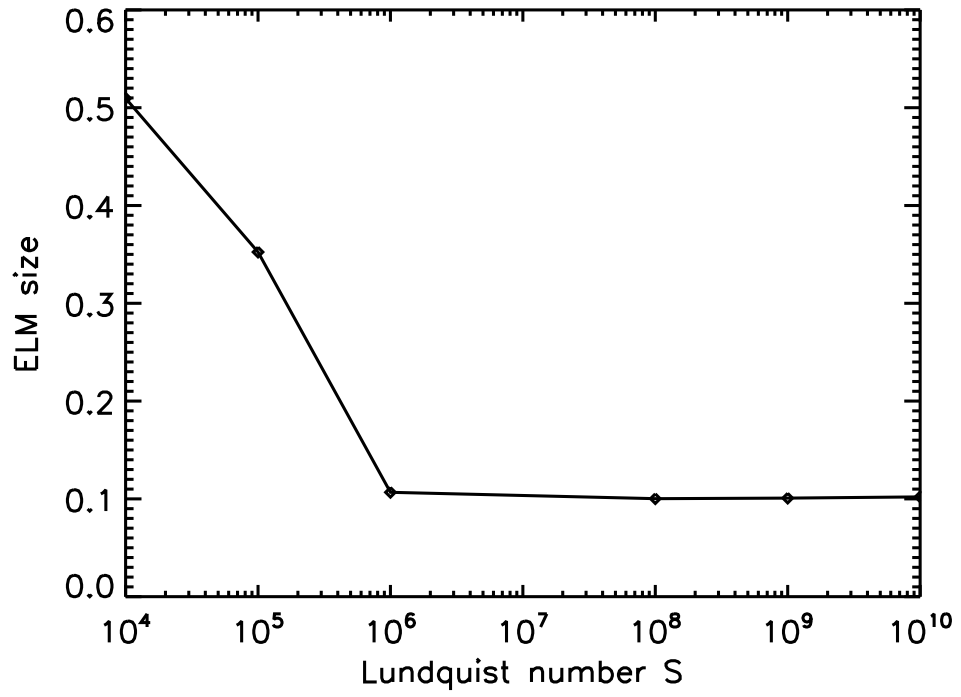


FIG. 4: Elm sizes vs Lundquist number S with $S_H = 10^{12}$.

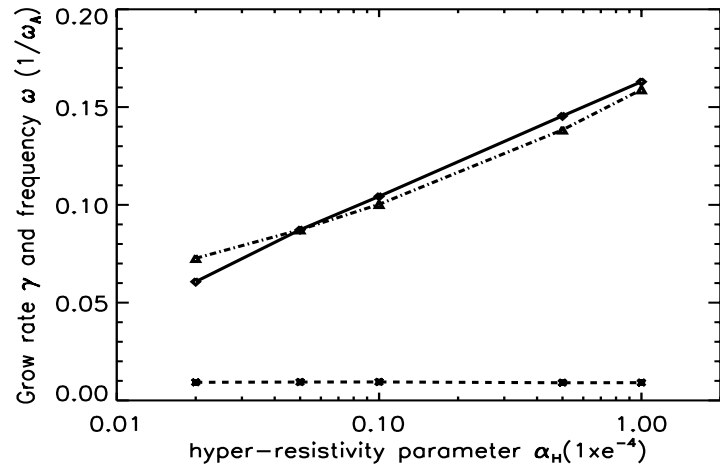
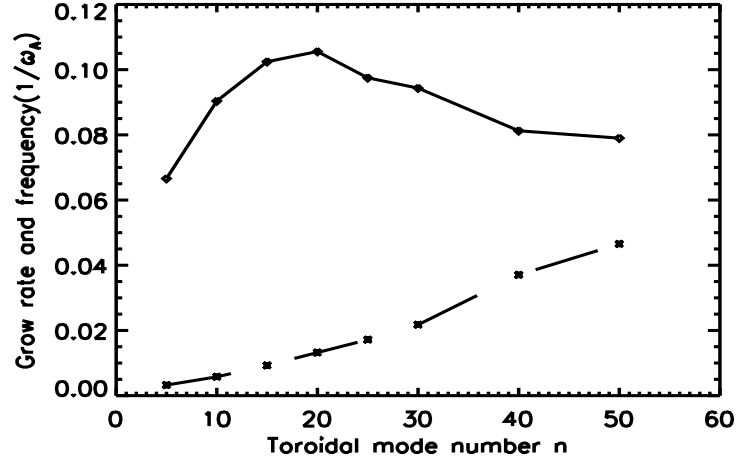


FIG. 5: (a) The linear growth rate of CDBM modes vs toroidal mode number n with diamagnetic drift and ExB drift. The solid line is growth rate and dashed line is frequency. (b) The linear growth rate of CDBM modes vs hyper-Lundquist parameter α_H with diamagnetic drift and ExB drift. The solid line is growth rate and dashed line is frequency.

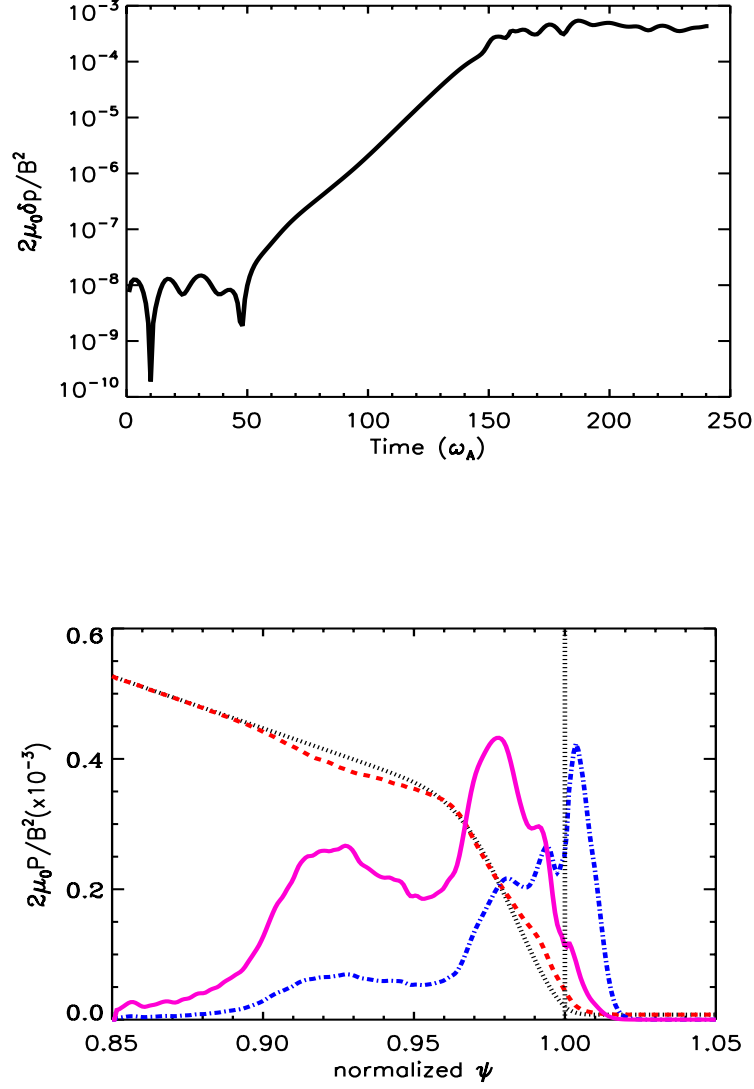


FIG. 6: (a) Time history of perturbed pressure $\langle \delta p \rangle_{rms}$ at outside-mid plane at the peak pressure gradient location. (b) Radial pressure profiles: the black dotted curve is initial pressure $P_0 (\times 10^{-2})$, the red dashed curve is the final pressure profile $P = P_0 + \delta p_{n=0}$ with $P (\times 10^{-2})$, the pink solid curve for perturbed pressure $\langle \delta p \rangle_{rms} (\times 10^{-3})$ and blue dotted curve for relative perturbed pressure $\langle \delta p \rangle_{rms}/P$. The vertical dotted line at $\psi = 1$ is the separatrix position.

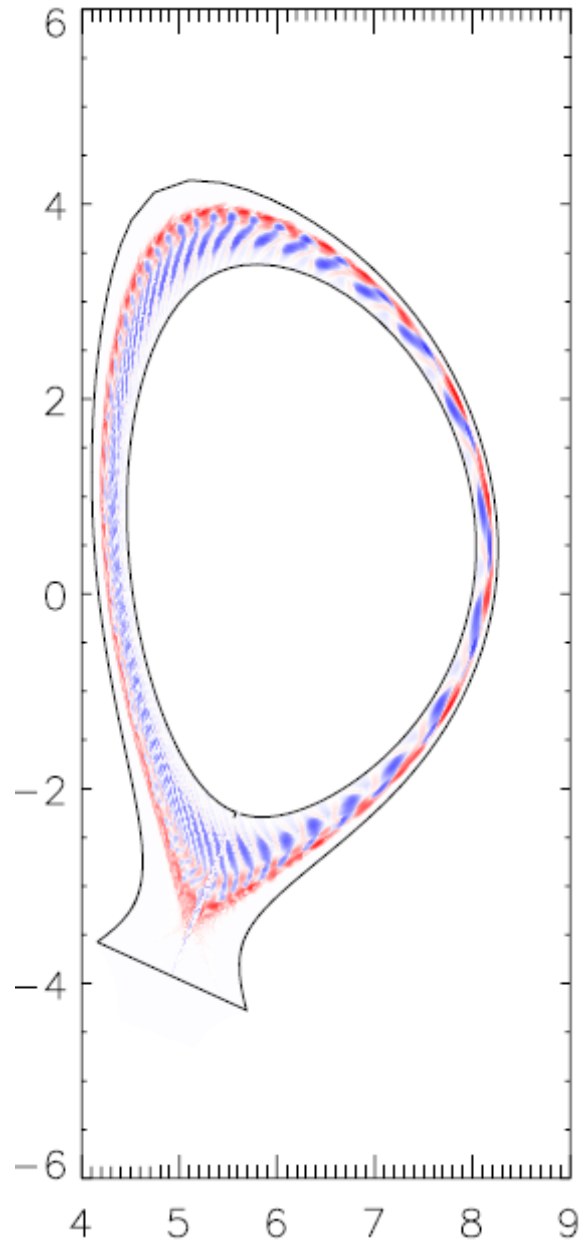


FIG. 7: Poloidal slice through the ITER H-mode plasma in single-null divertor configuration, showing pressure perturbation δp for dominant toroidal mode number $n = 15$ with the characteristics of ballooning mode.